Korean J. Chem. Eng., 40(12), 2965-2974 (2023)
DOI: 10.1007/s11814-023-1557-1

pISSN: 0256-1115
eISSN: 1975-7220

Experimental and factorial study on gas separation properties of PLA-based green composite membranes

Sedef Yüksel Yılmaz*, Hülya Aykaç Özen,†, and Feza Geyikçi***

*Department of Chemical Engineering, Ondokuz Mayis University, 55200, Samsun, Turkey
**Department of Environmental Engineering, Ondokuz MayisUniversity, 55200, Samsun, Turkey
(*Received 12 April 2023 • Revised 18 July 2023 • Accepted 24 August 2023*)

Abstract−Polylactide acid (PLA) is a biocompatible sustainable material with notable characteristics due to its good mechanical properties and low environmental impact. The present study investigated the effects of PLA-based green membranes on gas separation and identified the best factor condition for the membrane. Prepared membranes were tested to determine oxygen (O_2) and carbon dioxide (CO_2) gas permeability properties. Oxygen gas permeability of the PLA/PEG/HA membrane obtained by drying for two days was increased from 100 kPa to 400 kPa; the permeability value of this membrane increased by 15%. On the other hand, the oxygen permeability value of the membrane prepared by dry for three days under the same pressure conditions and ambient temperature increased by 5%. This result indicates that the permeabilities of prepared membranes for O_2 gas increase with increasing feed pressures. On the other hand, it was observed that the CO_2 permeability decreased by 38.83% with the increase in pressure and drying time due to the plasticizing and swelling effect of carbon dioxide on the membrane. A factorial design was also constructed from experimental data and applied to determine the interactions of experimental parameters. All of the parameter interactions were of statistical significance for permeability. It is further argued that molecular weight has a significant positive effect on permeability, while dry time and pressure have just a slight negative effect. This study could contribute to further studies by reducing the number of tests necessary to understand the characteristics and gas separation performance of green materials.

Keywords: Sustainable, Biodegradable, Greenhouse Gas, Gas Separation, Membrane, Experimental Design

INTRODUCTION

Increased consumption of petroleum-based products has resulted in significant petroleum crises due to the finite nature of fossil resources, the production of greenhouse gases, and the considerable waste of resources that has been rising rapidly [1-3]. Not only does that lead to a massive increase in the volume of waste, but this also contributes to the annual emission of millions of tons of CO_2 due to burning fossil resources. Therefore, biodegradable and biocompatible polymers are gaining popularity since they are environmentally friendly and can potentially substitute conventional composites generated from petroleum, commonly utilized in many fields [4-8]. Among biodegradable plastics, polylactide acid is the most widely used and fabricated by polymer stem from renewable sources in the literature because of its excellent attributes. such as good clarity, ease of manufacture, high tensile strength, biocompatibility, nontoxicity [9]. It also offers notable benefits, including low energy use and a decrease in the release of greenhouse gases into the atmosphere during manufacture [10,11]. However, PLA is still confined in application due to its poor mechanical characteristics and fragility, slow resorption period, low free surface energy, and hydrophobic surface trigger its usefulness in practice [12,13]. Considerable efforts have been made to prevent its usage restrictions and significantly improve mechanical properties. Studies have revealed that this issue can be achieved by combining PLA with the addition of ceramic nanomaterials. The fact that these substances increase bioactivity and have good stability under physical conditions makes it possible to achieve desired mechanical properties with the incorporation of PLA polymer gaining interest significantly. Persson et al. [14] studied the incorporation of hydroxyapatite (HA) particles and PLA to evaluate the effects of HA density on the vinculin in MC3T3-E1 surface. The presence of HA improved cell spreading and the structure of the fiber, suggesting PLA/HA composites have the potential to use bone as biomaterials. Laput et al. [15] manufactured polylactic acid/hydroxyapatite composite polymers in a 70/30 ratio by using plasma treatment to investigate the physicochemical properties of the surface. The characteristics of the polymer showed decreased water and improved free surface energy. Zimina et al. [16] fabricated a composite polymer, adding hydroxyapatite into polylactide acid polymer by solvent casting method. Compared to pure PLA scaffolds, HA-containing PLA demonstrated a less significant inflammatory response after two weeks of implantation. These findings indicate that PLA/HA composites have much potential for different fields. From previous research, Poly(ethylene glycol)monomethyl ether (mPEG) has been studied widely as an alternative polymer used in the preparation of polymer-protein conjugates because of its polymer biocompatibility and controlled biodegradability [17]. PEG has uncharged, soluble, nontoxic, and non-

†To whom correspondence should be addressed.
E-mail: hulya.aykac@omu.edu.tr

immunogenic properties and is an ideal material to protect active biomolecules due to its excellent properties [18]. Hence, adding mPEG into PLA/HA composite is predicted to enhance the characteristics of the composite, making it more suitable for membrane applications.

It is essential considering how different variables interact to affect the performance of a material structure. Design of experiments (DOE) is frequently used to investigate empirical relationships between one or more measured responses and a number of variables or factors [19]. In general, it helps organize the experimental documentation of a process by linking its independent variables (inputs) to the related responses. The design of the experiment, which minimizes the number of tests, costs, and time involved in performing the experiments, has been used by many researchers in their work [20,21]. A DOE has been employed in a number of engineering disciplines for optimization, including membrane technology. Moo-Tun et al. [22] used a full factorial design 2^3 to examine the impact of PLA, cellulose microfibers (CEL), and calcium carbonate ($CaCO_3$) on the equilibrium moisture content (EMC), density, and flexural mechanical characteristics of starch-based bio-foams. In another study, Watcharaprapapong et al. [23] reported PLA blends as a biocomposite material with 5-15% HA powder. The specimens were created via hot compression molding, and the experiment used a center point design with 2^3 full factorials to investigate the best conditions for creating the specimens.

To our best knowledge, the study of the incorporation of HA and PEG into PLA to manufacture environmentally friendly green composites and analyze their gas separation using an experimental factorial design has not been reported yet. In the present work, green biocomposites were developed and evaluated as substitutes for conventional composites. For this purpose, PLA/PEG/HA composites were prepared to achieve desired mechanical properties and examine the potential for gas separation. To produce PLA/PEG/HA composite, hydroxyapatite ceramic material and PEG included in PLA were produced by the sol-gel method, and composite materials were prepared by the solution casting method. The PEG and HA grafted onto PLA were confirmed by the results of surface infrared spectroscopy (FT-IR), scanning electron microscope (SEM), thermal gravimetric analysis (TGA), and differential scanning calorimetry (DSC). Gas separation measurements of manufactured composites were performed for CO_2 and O_2 gases. A full factorial model was implemented using statistical experiment design principles to study the impact of various parameters on gas separation.

MATERIALS AND METHODS

1. Sample Preparation

HA was synthesized by sol-gel method in the following order as mentioned in previous studies [24]. 100 mL of 0.6 M H_3PO_4 aqueous solution and 100 mL of 1 M $Ca(OH)_2$ ethanol solution were vigorously stirred at 60 °C for 4 hours. The mixed solutions were kept for 18 hours, and the phosphorus solution was added to the calcium hydroxide solution with a Ca/P ratio of 1.67 maintained by the stoichiometric ratio [25-27] and stirred for one more hour at 50 °C. The sample was heated in a muffle furnace at a rate of 5 °C/min up to 800 °C, kept there for 0-2 hours, and then put into air to cool to room temperature to obtain HA powder.

PLA, PEG, and HA powders were used to produce the biocomposite at weights of 86.96%, 10.87%, and 2.17%, respectively. The materials forming the biocomposite were mixed in solution (Fig. 1). The details for biocomposite synthesis are described elsewhere. Briefly, PLA and PEG powders were dispersed in chloroform for almost 1 hour, followed by adding the corresponding amount of HA powders, then stirred for approximately 24 hours at 120 rpm until it completely dissolved. Afterward, 10 ml of the mixture was cast onto the glass surface (Petri dishes), and the solvent was left to evaporate at room temperature for two days and three days. Membranes used in gas separation experiments have 100 μm thickness.

2. Samples Characterization

Characterization properties of synthesized PLA/PEG/HA composite films and produced hydroxyapatite were determined previously following the standard methods. Measurements were made in the wavelength range of 400-4,000 cm^{-1} using the Perkin Elmer, Spectrum Two, USA brand FT-IR/ATR device to determine the prepared membranes' chemical structures and obtain information about the bond structures. The thermal stability and thermal behavior of the prepared composite films were performed using a Shimadzu DTG-60 instrument. The film sample was coated with

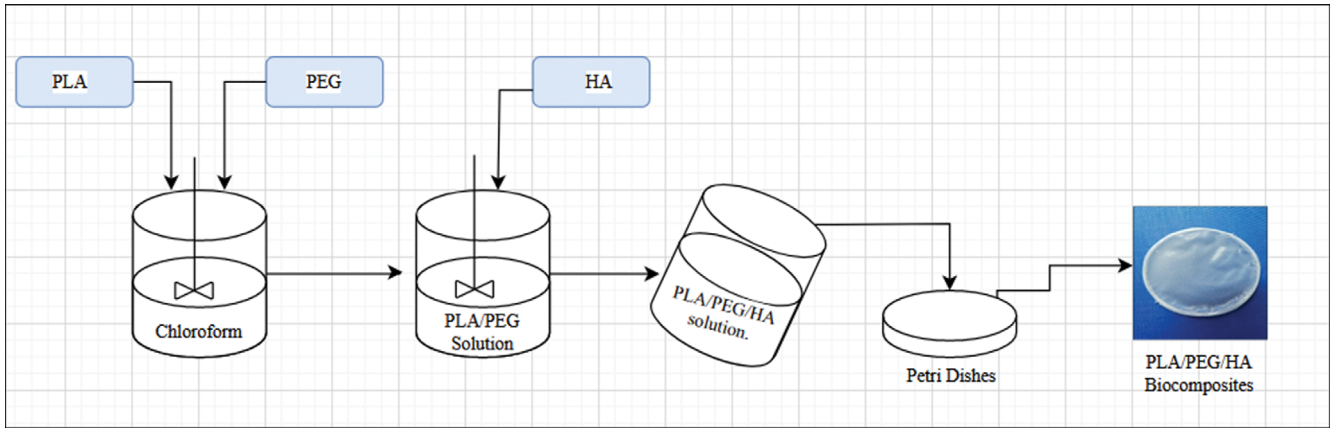

Fig. 1. Schematic procedures for the preparation of PLA/PEG/HA biocomposite.

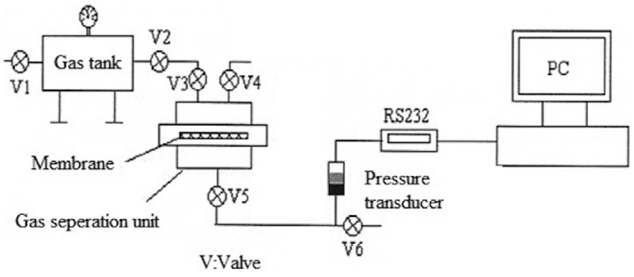

Fig. 2. Gas permeation unit.

alumina, and the measurement was taken by heating it from 25 °C to 500 °C at a heating rate of 10 °C/min in N_2 environment. Differential scanning calorimetry (DSC) analyses were carried out under a 10 °C/min heating rate between −30 °C and 300 °C to determine the thermal properties of the films such as glass transition temperature (Tg), crystallization temperature (Tc), melting point temperature (Tm), crystallization enthalpy (vHc), melting enthalpy (ΔHm) and percentage of crystallization (Xc). The morphologies of the samples were investigated using a JSM- 7001F field emission scanning electron microscope.

3. Gas Separation Experiment

Gas permeation performance involved using the variable pressure-constant volume method. The experimental setup consisted of a pressure indicator, pressure transducer, vacuum pump, computer, gas tank, and stainless steel gas separation unit presented in Fig. 2. Detailed information about the experimental design was reported in the literature [28]. The test cell's typical membrane area and permeate side volume were 49.2 cm^2 and 30.2 mL, respectively. By feeding at different pressures from the upper part of the membrane assembly, the pressure change of the gas passing to the bottom with the help of the pressure transducer was measured against time. Single gas permeability throughout the membranes was determined for O_2 and CO_2 gases at different pressures (100 and 400 kPa). All measurements were performed at room temperature.

The gas permeability (P) was calculated by the slope of the curve of permeate pressure vs. time (dp/dt) using the *Daynes-Barrier time lag* equation as follows [29].

$$P = \left(\frac{dp}{dt}\right)\frac{VT_0}{A\Delta P}\times\frac{L}{TP_0}$$

where P is the permeability coefficient, barrer (1 barrer=1×10^{-10} cm^3 cm/cm^2 s cmHg), dp/dt is slope of the line obtained in the permeability test, V is downstream volume (cm^3), ΔP is pressure difference between membrane surfaces (cmHg), A is membrane area (cm^2), L is membrane thickness (cm), T is room temperature (K), T_0 is standard temperature (K), P_0 is standard pressure (cmHg). The ratio of the permeation rates of pure gases A and B is known as the ideal separation factor of pure gas A over B (α_{AB}).

Table 1. Factors and levels used in the 2^3 factorial experimental design

Factor	Symbol	Low level (−1)	High level (+1)
Dry time (day)	A	2	3
Pressure (kPa)	B	100	400
Molecular weight (g)	C	32	44

4. Factorial Experimental Design

The experimental design is important to ensure the interaction and relationships between independent and dependent variables, a scientific and systemic approach. For finding parameters, a rank of interaction and effects was applied to the statistical software MINITAB 21. To investigate the gas permeability of PLA/PEG/HA composite through the O_2 and CO_2, an experimental design 2^3

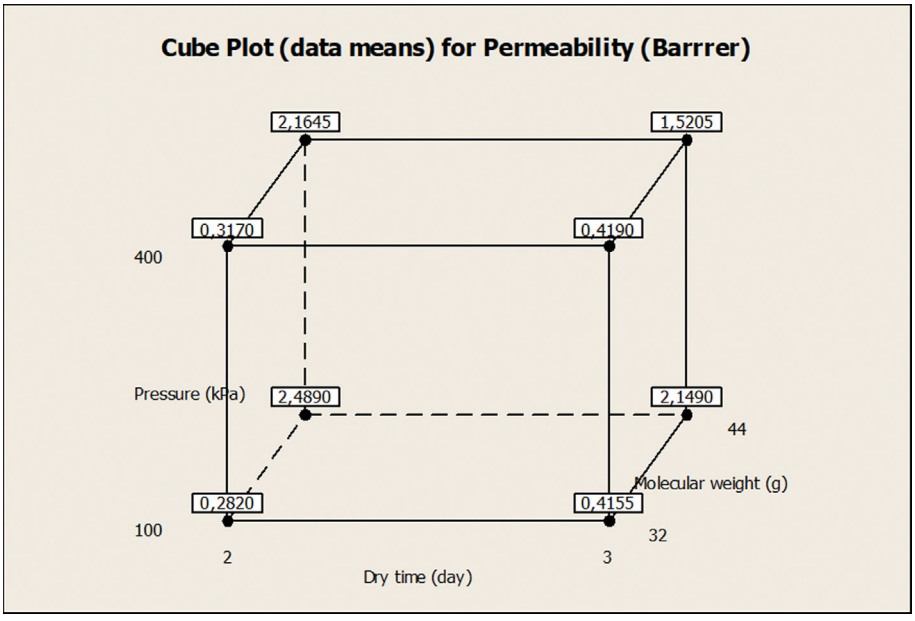

Fig. 3. Cube plots for permeability.

was carried out to study the influence of certain parameters. To evaluate the diffusion of O_2 and CO_2 gases from PLA/PEG/HA composite films, molecular weights, dry time, and pressure were selected as variables.

The 2^3 factorial experiments were applied on two levels, high and low. The factors and their two levels are given in Table 1.

The low and high levels of the factors were determined by considering some preliminary experiments [30]. The cubical diagram for high and low three independent variables (dry time, pressure, and molecular weight) is given in Fig. 3.

RESULTS AND DISCUSSION

1. Material Characterization

The peaks obtained from the FT-IR spectra of PLA, HA, PEG, and PLA/PEG/HA composites are shown in Fig. 4. The FT-IR spectra for the samples in the study were obtained in the region 600-4,000 cm^{-1}, and the spectrum showed three main regions. The absorption peaks at ~2,886 cm^{-1} are assigned to the CH stretching. The C=O stretching is observed as a large band at ~1,750 cm^{-1}, CH_3 band is observed at ~1,454 cm^{-1}. In the region of 1,300 cm^{-1} to 1,000 cm^{-1}, it is possible to observe the C-O stretching modes (~1,277, ~1,183, ~1,084), the ester groups at ~1,277 cm^{-1} and the nO-C asymmetric mode at ~1,084 cm^{-1} and -OH bending have the band at ~1,047 cm^{-1}. Between 1,000 cm^{-1} and 800 cm^{-1}, peaks can be observed at ~962 cm^{-1} and ~843 cm^{-1}, which can be attributed to the characteristic vibrations of the helical backbone with CH_3 rocking modes [31,32]. It is clear that the intensity for PLA/PEG is lower than PLA. The PLA/PEG combination shows less intensity in terms of C=O peaks, while HA does not contain the C=O peak.

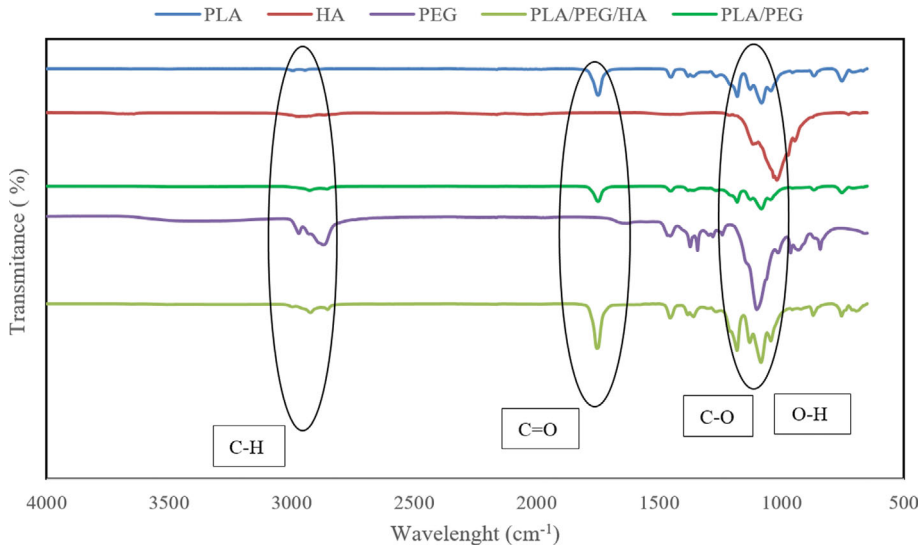

Fig. 4. FTIR analysis of PLA, HA, PEG, PLA/PEG, and PLA/PEG/HA.

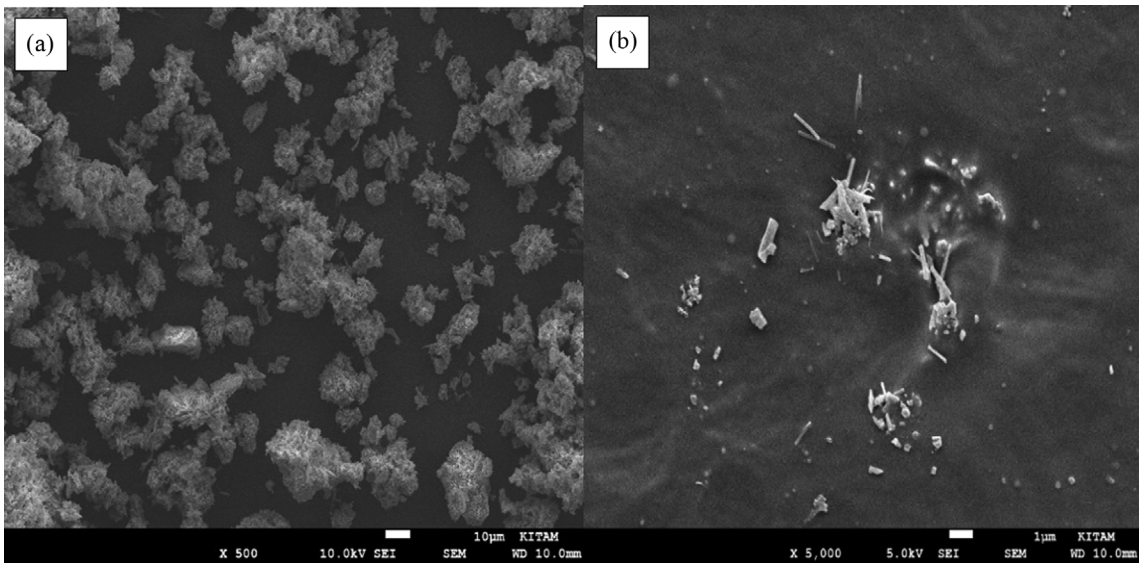

Fig. 5. (a) SEM images of Hydroxyapatite, (b) SEM images ofPLA/PEG/HA.

Thus, because PEG has a higher density than PLA, the density of the composite PLA/PEG film is likewise lower. PEG, in a sense, reduces the composite film's peak intensity. The peaks specific to pure PLA were also seen in the PLA/PEG structure when comparing the FTIR data of PLA and PLA/PEG. This can be explained by the fact that the peak intensity of one compound can be reduced or completely hidden by the stronger absorption of another compound. This result is consistent with the literature [33].

Fig. 5(a) exhibits that the HA has a surface appearance with a cluster-like and porous structure, which this same formation has been seen in numerous research in the literature [24]. The performance of the gas separation can be influenced by the PLA/PEG/HA membrane's surface morphology. For this reason, the distribution and compatibility of HA in the polymer matrix were observed using the SEM images of the top surface composite membrane (Fig. 5(b)). As can be observed in Fig. 5(b), PLA shows a very clean and smooth fracture surface due to its brittle behavior at room temperature. After the addition of HA, there are clear and evenly distributed structures on the PLA/PEG film's surface. Obviously, HA particles were uniformly dispersed in the composite membrane, and the distribution of HA in that film structure was in the form of regional clusters.

The results of thermal gravimetric analyses (TGA) of samples are given in Fig. 6. Pure PLA exhibits a two-stage weight loss in its composition. The first weight loss of 6.65% was due to the loss of guest molecules (solvent and adsorbed water) in the PLA structure between 88-138 °C. The second weight loss was observed between 316-374 °C, and pure PLA left a residue that was equal to zero. Because the PLA structure degrades in this temperature range, the initial value of this step (316 °C) determines the thermal stability of the structure. The weight loss values obtained at the first and second stages of the curve are consistent with the values reported in the literature [34]. The degradation of PLA/PEG is a two-step degradation process. It started at 234 °C and ended abruptly at 318 °C due to the removal of water and solvent molecules in its composition. The second step was associated with the degradation of PLA/PEG. The second weight loss occurred between 386-416 °C, and the mass loss at this stage was due to organic decomposition [35]. The thermal analysis curves show a three-stage weight loss in the case of PLA/PEG/HA membrane. First weight loss (about 5%) occurred before 200 °C, which can be ascribed to adsorbed water evaporation. The second weight loss (about 76%) occurred between 270 °C and 362 °C, and complete decomposition occurred between 364 °C and 410 °C. This represents the amount of char residue, 3.35 wt%, resulting from the formation of a carbonaceous char layer from the burning of hydroxyapatite incorporated in the composite [36]. The TGA curve of PLA/PEG/HA evidenced that the presence of HA had shown the potential to improve the thermal stability and resistance to the thermal degradation of a polymer [37].

The thermal properties of the samples are given in Table 2. With the addition of PEG and HA into PLA PLA/PEG/HA, the glass tran-

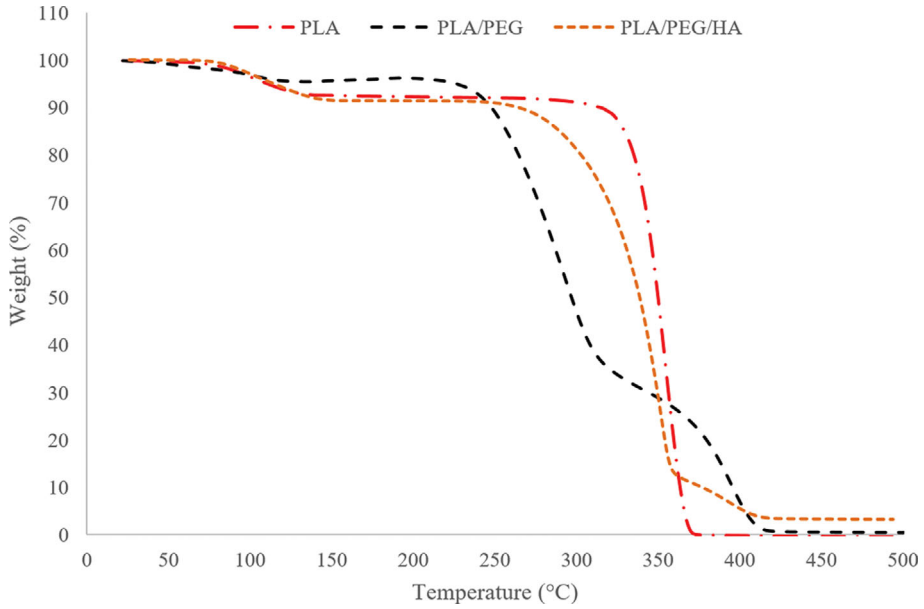

Fig. 6. TGA analysis of PLA, PLA/PEG, and PLA/PEG/HA.

Table 2. DSC results of PLA, PLA/PEG, and PLA/PEG/HA

	T_g (°C)	T_c (°C)	T_m (°C)	ΔH_m (J/g)	X_c (%)
PLA	59.4	123.56	149.48	16.27	17.38
PLA/PEG	-	75.33	147.14	25.81	34.47
PLA/PEG/HA	56.16	90.35	152.8	27.86	34,18

Table 3. Gas permeation and separation performances of PLA/PEG/HA

PLA/PEG/HA				
		Permeability, P *(Barrer)		Selectivity, α
Dry time	Pressure (kPa)	P_{O2}	P_{CO2}	$\alpha_{O2/CO2}$
2 days	100	0.280	2.488	0.113
	400	0.317	2.164	0.146
3 days	100	0.416	2.148	0.194
	400	0.418	1.522	0.275

sition temperature (T_g) decreased and the melting point temperature increased by about 3 °C compared to pure PLA membrane. In addition, the crystallization temperature (T_c) decreased by 36.75% when it formed PLA/PEG/HA structure. In DSC analysis, the percentage of crystallization in PLA/PEG/HA composites increased by 96.67% compared to PLA. This result indicates that the increase in the crystal structure in polymers decreases the mobility in the polymer chain in the presence of HA, which is consistent with previous studies [38].

2. PLA/PEG/HA Biodegradable Composite for O_2/CO_2 Separation

Separation of single gas (CO_2 and O_2) was investigated for PLA/PEG/HA Composite Films at different gas feed pressures (100 and 400 kPa). The permeability-selectivity results were summarized in Table 3 and discussed the effects of feed pressure (ΔP) and dry time of the membrane.

Oxygen permeability of the PLA/PEG/HA membrane was calculated as 0.280 and 0.317 barrer at pressures of 100 and 400 kPa for two days of drying and 0.416 and 0.418 barrer at the same pressures for three days drying, suggesting permeability increased with increasing drying time and pressure. Prepared membranes were also tested to determine the permeability properties of CO_2 gas. However, it was observed that the CO_2 permeability decreased from 2.488 barrer to 1.522 barrer with the increase in pressure and drying time due to the plasticizing and swelling effect of carbon dioxide on the membrane. This result is explained in the literature by the plasticizing effect of CO_2. Carbon dioxide has the potential to plasticize or swell the membranes, which reduces their separation effectiveness and results in a significant loss in selectivity under high feed pressures [39-41]. For instance, introducing CO_2 alters the viscosity of the polymer by plasticizing the molecules' movement through polymer swelling [42]. The crystallization kinetics was subsequently changed as a result [43,44]. Additionally, it has been demonstrated that the CO_2's plasticizing impact caused the crystallization temperature (T_c) and the glass transition temperature (T_g) to decrease as the dissolved CO_2 level increased. Previous research has mainly concentrated on how CO_2 affects the glass transition temperature (T_g), which has been demonstrated to decrease with increased pressure [45,46]. The effects of various gas pressures on the fluctuations in T_c of the polypropylene were investigated by Naguib et al. [47], who demonstrated that the T_c of polypropylene was reduced due to CO_2's plasticizing impact. Table 3 also indicates ideal O_2/CO_2 selectivities as a function of feed pressure and dry time. As the pressure and drying time increased, the ideal selectivity up to 0.275.

Table 4. Experimental design matrix and the results of the 2^3 full factorial design

Run No.	Factor			Permeability (Barrer)		
	A	B	C	Replicate		Average
				I	II	
1	−1	−1	−1	0.280	0.284	0.282
2	+1	−1	−1	0.416	0.415	0.416
3	−1	+1	−1	0.317	0.317	0.317
4	+1	+1	−1	0.418	0.420	0.419
5	−1	−1	+1	2.488	2.490	2.489
6	+1	−1	+1	2.148	2.150	2.149
7	−1	+1	+1	2.164	2.165	2.165
8	+1	+1	+1	1.522	1.519	1.521

Table 5. Estimated effects and coefficients for permeability

Term	Effect	Coef	SE Coef	T	p
Constant		1.2196	0.000390	3124.58	<0.001
A	−0.1871	−0.0936	0.000390	−239.71	0.000
B	−0.2286	−0.1143	0.000390	−292.87	0.000
C	1.7224	0.8612	0.000390	0.000390	0.000
A*B	−0.0839	−0.0419	0.000390	−107.45	0.000
A*C	−0.3049	−0.1524	0.000390	−390.55	0.000
B*C	−0.2479	−0.1239	0.000390	−317.53	0.000
A*B*C	−0.0681	−0.0341	0.000390	−87.27	0.000

S=0.00156127R-Sq=100.00% R-Sq(pred)=100.00%R-Sq(adj)=100.00%

3. Factorial Design Study

In this study, factorial design experiments were applied to analyze the gas permeability of PLA/PEG/HA composite films against the O_2 and CO_2. The effective factors on the gas permeability of PLA/PEG/HA composite films are the dry time, pressure, and molecular weight. Three different input independent variables of values and the responses of the process with 2^3 full factorial design were given in Table 4.

The results of experimental data were analyzed with the MINITAB 21 software. The effect, regression coefficients (coef), standards errors (SE coef), T, and p-value are given in Table 5.

The T-value indicates the size of the difference in relation to the variability in the sampled data and also stands for the simply calculated difference expressed in standard error units. The p-value represents the probability that the results derived from the sample data are the result of chance. p-values range from 0% to 100% and are typically expressed as decimal numbers (For instance, a p value of 5% is 0.05) and can have any value between 0 and 1 because it is a probability. Values that are close to 0 show that it is improbable that the observed difference is the result of chance.

An empirical model using the regression coefficients was given for permeability in Eq. (1). It was observed that the linear effect of all factors and the interaction effect between these factors are significant.

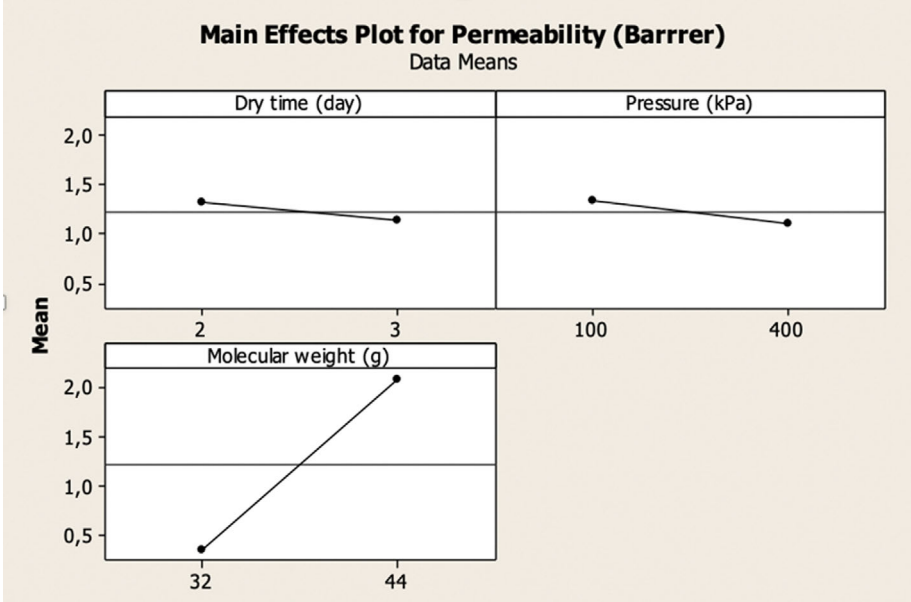

Fig. 7. Main effect graphs for permeability.

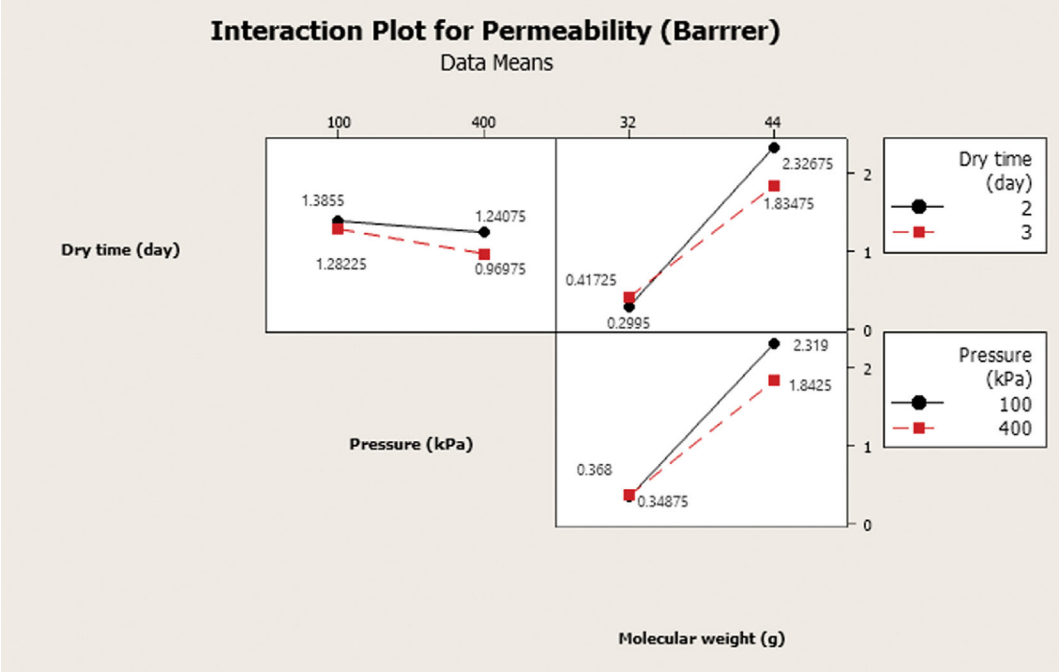

Fig. 8. Interaction effects graphs for permeability.

$$qe = 1.2196 - 0.0936A - 0.1143B + 0.8612C - 0.0419AB - 0.1524AC - 0.1239BC - 0.0341ABC \quad (1)$$

The positive values of these effects reveal that the increase of these independent variables increased permeability. Conversely, negative values of the effects decreased the permeability.

The main effects represent the deviation of the mean values between the low and high levels. These graphs were generated to describe the results of the regression analysis. When the effect of a factor is positive, permeability increases as the factor changes from low to high levels. In contrast, if the effects are negative, a reduction in permeability occurs for a high level of the same factor [48]. As stated in Fig. 7, whereas dry time and pressure have a very weak negative effect on permeability, molecular weight has a strong positive influence on permeability. Maximum permeability occurred at the high molecular weight.

An interaction plot is a powerful graphical tool that the interaction between the components is not possible if the lines on the interaction plot are parallel. The probability of an interaction between the lines increases if they intersect [48,49]. Interaction effects graphs

Table 6. Analysis of variance for permeability

Source	Degree of freedom	Sum of squares (SS)	Mean squares (SS)	F	p
Main effects	3	12.2154	4.0718	1670487.96	0.000
A	1	0.1401	0.1401	57461.77	0.000
B	1	0.2091	0.2091	85775.41	0.000
C	1	11.8663	11.8663	4868226.69	0.000
2-Way Interactions	3	0.6457	0.6457	88301.29	0.000
AB	3	0.0281	0.2152	88301.29	0.000
AC	1	0.3718	0.0281	11544.64	0.000
BC	1	0.2458	0.3718	152531.31	0.000
3-Way interactions	1	0.0186	0.0186	7616.03	0.000
ABC	1	0.0186	0.0186	7616.03	0.000
Residual error	8	0.0000	0.0000		
Pure error	8	0.0186	0.0000		
Total	15	12.8797			

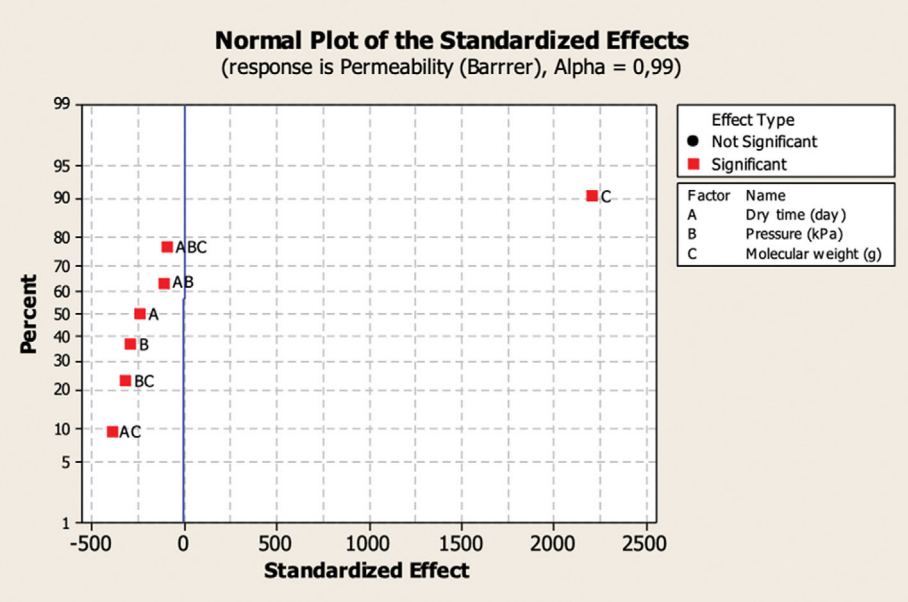

Fig. 9. Normal probability graph of standardized effects for permeability.

for permeability are shown in Fig. 8. It reveals that all the interactions of the factors were statistically significant in determining permeability. The permeability decreased by 10.45% with the increase in pressure from 100 kPa to 400 kPa during two days of drying, whereas the permeability decreased by 24.37% with the same pressure increase in three days of drying time. This indicated that permeability in two day-dry time has a greater effect positively. When analyzing the interaction plot of pressure and molecular weight, the result indicated that pressure and molecular weight are in interaction with each other. At 100 kPa pressure, 84.13% increase in permeability is observed when from low molecular weight to high molecular weight, while the increase in this value is 81.07% at 400 kPa pressure. Similary, the dry time and molecular weight interaction plot illustrates that permeability increase by 87.13% the during two days of drying from lower molecular weight to higher molecular weight, and also during three days of dry time led to a rise in permeability by 83.68% under same conditions. It could be seen that there is an interaction between dry time and molecular weight.

Table 6 presents the sum of squares used to estimate the factor effects and *F*-rations. *p* values i ndicate that the effects are statistically significant. The significance of the regression coefficients was determined by applying the Student's *t*-test. All effects were significant, with a 95% confidence level. In addition, the coefficients of the model, interaction and main effect, probability, and standard deviation of each coefficient for the 2^3 factorial design are presented Table 6.

The normal probability graph of standardized effects is given in Fig. 9. In this graph the statistically significant effects are characterized by square signs situated away from the center line; however, the circle signs representing the insignificant effects tend to follow a normal distribution. According to Fig. 9, a sign close to a line fitted to the middle group of points represents those estimated fac-

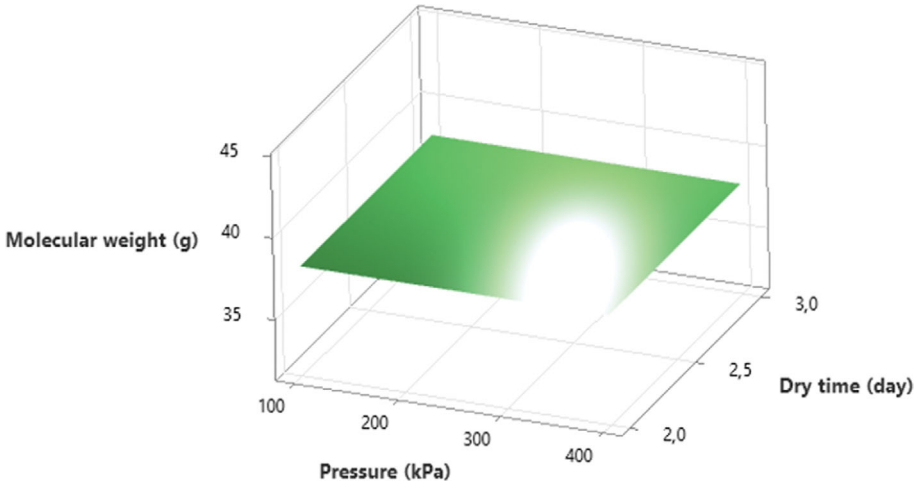

Fig. 10. 3D surface plot of molecular weight (g) vs. dry time (day) vs. pressure (kPa).

tors that do not demonstrate any significant effect on the response variables. Points far away from the line represent the "real' factor effects [30].

The molecular weight and their interaction are very far from the straight line and therefore considered "real". Because A, B, AC, BC, and AB lie to the left of the line, their contribution has a negative effect, and C represents molecular weight on the right had a positive effect, as seen in Fig. 9. A three-dimensional surface plot of Molecular weight (g) vs. Dry time (day) vs Pressure (kPa) is illustrated in Fig. 10.

This graph is used to visualize and understand the relationships between these three variables. It is a type of graph in which each variable is placed on the axis, and the surfaces of the graph are formed by the combination of these variables [50]. Also, it can be used to understand how the relationships between the variables molecular weight (g), drying time (days), and pressure (kPa) change and how they interact with each other. For example, it can be understood how drying time is affected as molecular weight increases or how pressure change affects molecular weight and drying time. It allows a specific value (e.g., the value of pressure and drying time at which the maximum molecular weight is reached) to be visually identified on the graph. As revealed formerly, increasing pressure from 100 to 400 kPa and molecular weight from 32 to 44 g enhances membrane permeability significantly.

CONCLUSION

Bio-membrane from renewable sources used for gas separation is a substantial research field regarding the issue of increasing greenhouse gas and petroleum-based waste. PLA is the most widely used and manufactured biodegradable polymer because of its excellent attributes over petroleum-based membrane. In this study, PLA was combined with HA and PEG to improve mechanical characteristics and biocompatibility. First, the effect of PLA/PEG/HA on morphological, mechanical performance, and gas separation performance was investigated. The effective incorporation of HA and PEG into the PLA structure was confirmed by FTIR studies of the composite. Because PLA has a higher density than PEG, the density of the composite PLA/PEG film is likewise lower. PEG reduces the composite film's peak intensity. The intensity of PLA was found to be higher than PLA/PEG because PEG decreased the peak intensity of the membrane.

HA particles were uniformly dispersed in the composite membrane, and the distribution of HA in that film structure was in the form of regional clusters. The PLA/PEG/HA TGA curve demonstrated that adding HA could potentially increase a membrane's thermal stability and resistance to thermal degradation. The PLA/PEG/HA membrane's oxygen permeability was calculated to be 0.280 and 0.317 barrer at pressures of 100 and 400 kPa that were conducted for two days and 0.416 and 0.418 barrer at the same pressures for three days, respectively. This suggests that permeability increases with both drying time and pressure. A prepared membrane's ability to permeabilize CO_2 gas was found that the plasticizing effects of carbon dioxide on the membrane caused the CO permeability to decrease from 2.488 barrer to 1.522 barrer with the rise in pressure and drying time. This result supports that the membranes may plasticize in response to carbon dioxide, which lessens their separation efficiency. The factorial design methodology has been applied successfully to determine the interactions of experimental parameters on gas permeability. Analysis showed that the interaction of dry time, molecular weight and pressure was statistically significant. The normal probability graph of standardized effects indicated that a positive effect can be seen by molecular weight. A higher permeability was found to be two days dry time, 100 kaPa pressure, and carbon dioxide gas with a molecular weight of 44 g/mol. The maximum permeability value was achieved by 87.13% at two days of drying and higher molecular weight. In brief, this study could help future research to understand the properties and gas separation performance of green materials and to determine the interactions of experimental parameters by minimizing the number of experiments.

ACKNOWLEDGEMENTS

The authors gratefully acknowledge Ondokuz Mayis University for the financial support through the project numbered as PYO.

MUH.1901.18.003.

DECLARATION OF COMPETING INTERESTS

The authors declare that they have no known competing financial interests or personal relationships that could have influenced the work reported in this study.

AUTHOR CONTRIBUTION

Sedef Yüksel Yılmaz: investigation, methodology, analyzing data and writing. Hülya Aykaç Özen: writing—original draft preparation, formal analysis, investigation, conceptualization, resources and review. Feza Geyikçi: methodology, investigation, analyzing data and review. All authors read and approved the final manuscript.

REFERENCES

1. A. M. Aitani, *Encyclopedia of Energy*, **4**, 715 (2004).
2. R. Liu, R. N. Jadeja, Q. Zhou and Z. Liu, *Environ. Eng. Sci.*, **29**, 494 (2012).
3. P. K. Bajpai, I. Singh and J. Madaan, *J. Thermoplast. Compos. Mater. J.*, **27**, 52 (2014).
4. E. L. Sánchez-Safont, A. Aldureid, J. M. Lagarón, J. Gámez-Pérez and L. Cabedo, *Compos. B. Eng.*, **145**, 215 (2018).
5. Vinod, M. R. Sanjay, S. Suchart and P. Jyotishkumar, *J. Clean. Prod.*, **258**, 120978 (2020).
6. M. Jamshidian, E. A. Tehrany, M. Imran, M. Jacquot and S. Desobry, *Compr. Rev. Food Sci. Food Saf.*, **9**, 552 (2010).
7. V. M. A. Valantin, C. Aubron-Olivier, J. Ghosn, E. Laglenne, M. Pauchard, H. Schoen and C. Katlama, *Aids*, **17**, 2471 (2003).
8. S. Ahmed, S. Ikram, S. Kanchi and K. Bisetty (Eds.), *Biocomposites: biomedical and environmental applications*, CRC Press (2018).
9. B. Gupta, N. Revagade and J. Hilborn, *Prog. Polym. Sci.*, **32**, 455 (2007).
10. F. La Mantia and M. Morreale, *Compos. - A: Appl. Sci.*, **42**, 579 (2011).
11. V. Mazzanti and F. Mollica, *Polym. Compos.*, **40**, E169 (2019).
12. Z. Ma, C. Gao, J. Ji and J. Shen, *Eur. Polym. J.*, **38**, 2279 (2002).
13. R. Auras, B. Harte and S. Selke, *Macromol. Biosci.*, **4**, 835 (2004).
14. M. Persson, G. S. Lorite, H. E. Kokkonen, S. W. Cho, P. P. Lehenkari, M. Skrifvars and J. Tuukkanen, *Colloids Surf. B*, **121**, 409 (2014).
15. O. Laput, I. Vasenina, M. C. Salvadori, K. Savkin, D. Zuza and I. Kurzina, *J. Mater. Sci.*, **54**, 11726 (2019).
16. A. Zimina, F. Senatov, R. Choudhary, E. Kolesnikov, N. Anisimova, M. Kiselevskiy and A. Karyagina, *Polymers*, **12**, 2938 (2020).
17. S. Essa, J. M. Rabanel and P. Hildgen, *Eur. J. Pharm. Biopharm.*, **75**, 96 (2010).
18. S. Momeni, E. Rezvani Ghomi, M. Shakiba, S. Shafiei-Navid, M. Abdouss, A. Bigham and S. Ramakrishna, *Polymers*, **13**, 1019 (2021).
19. M. Nele, A. Vidal, D. L. Bhering, J. C. Pinto and V. M. M. Salim, *Appl. Catal.*, **178**, 177 (1999).
20. S. Sadudeethanakul, W. Wattanutchariya, W. Nakkiew, A. Chaijaruwanich and S. Pitjamit, *OP Conf. Ser.: Mater. Sci. Eng.*, **635**, 012004 (2019).
21. B. C. Y Lee, M. S. Mahtab, T. H. Neo, I. H. Farooqi and A. Khursheed, *Water Process. Eng.*, **47**, 102673 (2022).
22. N. M. Moo-Tun, G. Iñiguez-Covarrubias and A. Valadez-Gonzalez, *Polym. Test.*, **86**, 106482 (2020).
23. P. Watcharaprapapong, W. Nakkiew, W. Wattanuchariya and S. Pitjamit, *MATEC Web Conf.*, **192**, 01049 (2018).
24. W. Zhang, N. Cao, Y. Chai, X, Xu and Y. Wang, *Ceram. Int.*, **40**, 16061 (2014).
25. M. Fathi and A. Hanifi, *Mater. Lett.*, **61**, 3978 (2007).
26. S. Waheed, M. Sultan, T. Jamil and T. Hussain, *Mater. Today: Proc.*, **2**, 5477 (2015).
27. M. Robles-Águila, J. Reyes-Avendaño and M. Mendoza, *Ceram. Int.*, **43**, 12705 (2017).
28. H. A. Ozen and B. Ozturk, *Sep. Purif. Technol.*, **211**, 514 (2019).
29. R. Lin, *MOFs-based mixed matrix membranes for gas separation*, Doktoral Thesis, The University of Qeensland, Australia (2016).
30. D. Bingol, N. Tekin and M. Alkan, *Appl. Clay Sci.*, **50**, 315 (2010).
31. B. W. Chieng, N. A. Ibrahim, W. M. Z. Wan Yunus, M. Z. Hussein, Y. Y. Then and Y. Y. Loo, *Polymers*, **6**, 2232 (2014).
32. M. A. Cuiffo, J. Snyder, A. M. Elliott, N. Romero, S. Kannan and G. P. Halada, *Appl. Sci.*, **7**, 579 (2017).
33. Y. Xiao, D. Li, H. Fan, X. Li, Z. Gu and X. Zhang, *Mater. Lett.*, **61**, 59 (2007).
34. K. M. Choi, S. W. Lim, M. C. Choi, Y. M. Kim, D. H. Han and C. S. Ha. *Polym. Bull.*, **71**, 3305 (2014).
35. A. Angelopoulou, E. Voulgari, E. K. Diamanti, D. Gournis and K. Avgoustakis, *Eur. J. Pharm. Biopharm.*, **93**, 18 (2015).
36. R. H. A Haq, O. M. F Marwah, M. N. A. Rahman, F. H. Ho, H. Abdullah, S. Ahmad and M. Z. Yunos, *Int. J. Integr. Eng.*, **10**, 187 (2018).
37. X. Zhang, Y. Li, G. Lv, Y. Zuo and Y. Mu, *Polym. Degrad. Stab.*, **91**, 1202 (2006).
38. J. Zhang, S. Wang, D. Zhao, Y. Zhang, W. Pang, B. Zhang and Q. Li, *J. Appl. Polym. Sci.*, **134**, 45194 (2017).
39. J. D. Wind, D. R. Paul and W. J. Koros, *J. Membr. Sci.*, **228**, 227 (2004).
40. A. M. Hillock and W. J. Koros, *Macromolecules*, **40**, 583 (2007).
41. A. M. Kratochvil and W. J. Koros, *Macromolecules*, **41**, 7920 (2008).
42. Y. Li and C. Park, *Ind. Eng. Chem. Res.*, **48**, 6633 (2009).
43. M. Mihai, M. A. Huneault and B. D. Favis, *J. Appl. Polym. Sci.*, **113**, 2920 (2009).
44. L. Yu, H. Liu and K. Dean, *Polym. Int.*, **58**, 368 (2009).
45. M. Nofar, A. Tabatabaei and C. B. Park, *Polymer*, **54**, 2382 (2013).
46. D. C. Li, T. Liu, L. Zhao, X. S. Lian and W. K. Yuan, *Ind. Eng. Chem. Res.*, **50**, 1997 (2011).
47. H. E. Naguib, C. B. Park, S. W. Song, *Ind. Eng. Chem. Res.*, **44**, 6685 (2005).
48. V. Ponnusami, V. Krithika, R. Madhuram and S. N. Srivastava, *J. Hazard. Mater.*, **142**, 397 (2007).
49. S. Saadat and A. Karimi-Jashni, *J. Chem. Eng.*, **173**, 743 (2011).
50. D. C. Montgomery, *Design and analysis of experiments*, John Wiley & Sons (2017).